Inorganic Chemistry

ARTICLE

pubs.acs.org/IC

Effect of Counteranion X on the Spin Crossover Properties of a Family of Diiron(II) Triazole Complexes $[Fe^{II}_2(PMAT)_2](X)_4$

Jonathan A. Kitchen,[†] Nicholas G. White,[†] Guy N. L. Jameson,[†] Jeffery L. Tallon,[‡] and Sally Brooker*[,†]

[†]Department of Chemistry and The MacDiarmid Institute for Advanced Materials and Nanotechnology, University of Otago, P.O. Box 56, Dunedin 9054, New Zealand

[‡]MacDiarmid Institute for Advanced Materials and Nanotechnology, Industrial Research Limited, P.O. Box 31310, Lower Hutt, New Zealand

Supporting Information

ABSTRACT: Seven diiron(II) complexes, $[Fe^{II}_2(\mathbf{PMAT})_2](X)_4$, varying only in the anion X, have been prepared, where **PMAT** is 4-amino-3,5-bis{[(2-pyridylmethyl)-amino]methyl}-4*H*-1,2,4-triazole and X = BF_4^- (**1**), Cl^- (**2**), PF_6^- (**3**), SbF_6^- (**4**), $CF_3SO_3^-$ (**5**), $B(PhF)_4^-$ (**6**), and $C_{16}H_{33}SO_3^-$ (**7**). Most were isolated as solvates, and the microcrystalline ([**3**], [**4**]·**2H$_2$O**, [**5**]·**H$_2$O**, and [**6**]·$^1/_2$**MeCN**) or powder ([**2**]·**4H$_2$O**, and [**7**]·**2H$_2$O**) samples obtained were studied by variable-temperature magnetic susceptibility and Mössbauer methods. A structure determination on a crystal of [**2**]·**2MeOH·H$_2$O**, revealed it to be a [LS-HS] mixed low spin (LS)-high spin (HS) state dinuclear complex at 90 K, but fully high spin, [HS-HS], at 293 K. In contrast, structures of both [**5**]·$^3/_4$**IPA·H$_2$O** and [**7**]·**1.6MeOH·0.4H$_2$O** showed them to be [HS-HS] at 90 K, whereas magnetic and Mössbauer studies on [**5**]·**H$_2$O** and [**7**]·**2H$_2$O** revealed a different spin state, [LS-HS], at 90 K, presumably because of the difference in solvation. None of these complexes undergo thermal spin crossover (SCO) to the fully LS form, [LS-LS]. The PF_6^- and SbF_6^- complexes, **3** and [**4**]·**2H$_2$O**, appear to be a mixture of [HS-LS] and [HS-HS] at low temperature, and undergo gradual SCO to [HS-HS] on warming. The $CF_3SO_3^-$ complex [**5**]·**H$_2$O** undergoes gradual, partial SCO from [HS-LS] to a mixture of [HS-LS] and [HS-HS] at $T_{1/2} \approx 180$ K. The $B(PhF)_4^-$ and $C_{16}H_{33}SO_3^-$ complexes, [**6**]·$^1/_2$**MeCN** and [**7**]·**2H$_2$O**, are approximately [LS-HS] at all temperatures, with an onset of gradual SCO with $T_{1/2} > 300$ K.

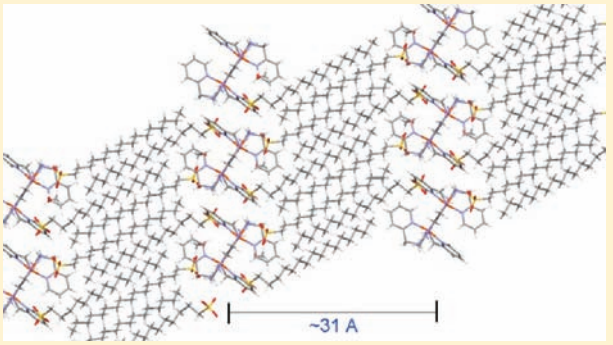

INTRODUCTION

The incorporation of the 1,2,4-triazole moiety in iron(II) spin crossover (SCO) complexes has been well documented.[1,2] Such triazole-based ligands often possess field strengths that lie within the right region to facilitate temperature-mediated switching between the high spin (HS) and low spin (LS) states of the iron(II) centers.[2] Many factors can influence the nature of the transition between the HS and LS states, for example choice of ligand substituents,[3,4] counteranions,[4−6] and/or reaction/recrystallization solvent(s). These and other factors are all important as they can affect the precise nature of the product, for example, whether or not interstitial solvent is present,[4,5,7] how extensive the intermolecular interactions are, and what crystal morphology is obtained. In turn, these are important as crystal packing effects are increasingly recognized as often being *the* critical factor controlling the exact nature of the SCO event.[7,8] Predictive control over the packing amounts to crystal engineering, a challenge that, for general cases, is yet to be met. Hence, attempts to systematically tune SCO, for example, the observed $T_{1/2}$, are ambitious; however, they are also necessary if we are to move from good luck to good management of SCO behavior, something which practical applications will demand.[9]

The dinuclear iron(II) complex $[Fe_2(\mathbf{PMAT})_2](BF_4)_4$·DMF (**1**) (**PMAT** = 4-amino-3,5-bis{[(2-pyridylmethyl)amino]methyl}-4*H*-1,2,4-triazole, Scheme 1) exhibits a thermally induced SCO at 224 K from the fully [HS-HS] state to the mixed [HS-LS] state.[10−12] That the [HS-LS] state comprises one HS and one LS iron(II) within each dimetallic complex, not a 1:1 mixture of [HS-HS] and [LS-LS] complexes, was confirmed by both single crystal X-ray diffraction (a first)[10] and standard VT Mössbauer spectroscopy studies (also a first, as usually an applied magnetic field is required).[11] The surprising stability of this [HS-LS] state was demonstrated through VT magnetic studies carried out on the sample under high pressure which showed no evidence of the [LS-LS] state, even at 10.3 kbar.[12] This dinuclear SCO active complex, with these intriguing magnetic properties, has provided us with an ideal base from which to further explore. For example, subtle changes to the system may facilitate tuning of the SCO

Received: February 14, 2011
Published: April 20, 2011

Scheme 1. Previous (Left)[13] and New (Right) Methods of Preparing PMAT

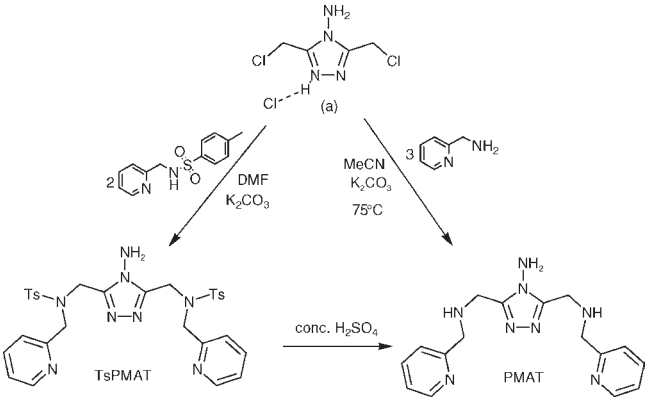

transition temperature, or perhaps even the observation of a fully low spin [LS-LS] state.

The present study focuses on perturbation of the magnetic properties of $[Fe^{II}_2(\mathbf{PMAT})_2]^{4+}$ through changing the counteranion, X, a change that has been documented to significantly alter SCO properties in mononuclear iron(II) systems.[4−6] Dinuclear iron(II) systems, however, have been studied far less with respect to such systematic changes. To generate a family of closely related complexes, $[Fe^{II}_2(\mathbf{PMAT})_2]X_4$, (preferably varying only in the choice of X) a common solvent and synthetic strategy is highly desirable. However, the solubility/reactivity of starting materials (ligand and/or metal salt) can preclude this. Such synthetic variations can affect the magnetic properties of the complexes obtained, so establishing trends is often not as easy as one might presume. Despite these challenges we are now actively exploring such systematic studies, and here report the results of varying the anion X, generating a family of seven $[Fe^{II}_2(\mathbf{PMAT})_2]X_4$ complexes. Where possible we have tried to eliminate synthetic variations by isolating complexes in one common solvent or solvent mixture; however, this was not always possible and any such variation is noted.

RESULTS AND DISCUSSION

Counter Anion (X) Selection. The counteranions used in this study were all mononegative; thus, all seven of the complexes, $[Fe^{II}_2(\mathbf{PMAT})_2](X)_4$, have four counteranions. The anions selected for this study included the monatomic chloride anion (Cl^-); bulky fluorinated species, hexafluoro phosphate (PF_6^-), hexafluoro antimonate (SbF_6^-), and trifluoromethanesulfonate ($CF_3SO_3^-$); and anions containing large organic groups, tetra-(4-fluoro)phenyl borate ($B(PhF)_4^-$) and hexadecyl sulfonate ($C_{16}H_{33}SO_3^-$). The complexes therefore had the general formula $[Fe^{II}_2(\mathbf{PMAT})_2]X_4$ where X = Cl^- (**2**), PF_6^- (**3**), SbF_6^- (**4**), $CF_3SO_3^-$ (**5**), $B(PhF)_4^-$(**6**), and $C_{16}H_{33}SO_3^-$ (**7**).

Ligand and Complex Synthesis. PMAT was prepared using a modification of the literature procedure[13] (Scheme 1). Previously, this involved first isolating the protected ligand, **TsPMAT**, followed by removal of the tosyl groups via acid hydrolysis to give pure **PMAT**.[13] Recently, however, we have had success in isolating **PMAT** without employing protecting groups and **TsPMAT**. Now, rather than using a tosyl protected amine to react with 3,5-bis-chloromethyl-4-amino-1,2,4-triazolium hydrochloride (Scheme 1, a), we conveniently use 3 equiv of 2-aminomethylpyridine, which results in a crude mixture of **PMAT** and unreacted primary amine. Following column chromatography (alumina, 5:1 EtOH/MeOH), to remove the majority of the excess primary amine, the resulting orange oil was used for complexation without further purification.

The synthesis of $[Fe^{II}_2(\mathbf{PMAT})_2](BF_4)_4$, **1**, has also been modified, to give slightly improved yields, and is detailed in the Experimental Section. Preparation of the six new complexes, **2**−**7**, involved either of the following:

(a) reacting **PMAT** in methanol with the desired iron(II) salts (**2** - $FeCl_2$, and **7** - $[Fe(OH_2)_4(C_{16}SO_3)_2]$[14,15]) or

(b) dissolving **1** in water and adding a slight excess of the sodium or ammonium salt of the desired anion (**3** - NH_4PF_6, **4** - $NaSbF_6$, **5** - $NaCF_3SO_3$, **6** - $NaB(PhF)_4$).

Five of these complexes (the exception is complex **5**) formed from one of these two protocols, **2** and **7** via (a) and **3**−**6** via (b). Interestingly, **3**−**6** could not be prepared via (a) and neither could **2** and **7** be prepared via (b). In all five cases the result was a pale powder that was filtered, dried in vacuo and then dissolved in MeCN/DMF (4:1) before being subjected to vapor diffusion of diethyl ether. Hence, as desired, a common recrystallization protocol was employed for these five complexes. Most of them were isolated as solvates, and the crystalline/microcrystalline ([**3**], $[\mathbf{4}]\cdot\mathbf{2H_2O}$, and $[\mathbf{6}]\cdot{}^1/_2\mathbf{MeCN}$) or powder ($[\mathbf{2}]\cdot\mathbf{4H_2O}$ and $[\mathbf{7}]\cdot\mathbf{2H_2O}$) samples, obtained after air drying, were fully characterized. All except complex $[\mathbf{2}]\cdot\mathbf{4H_2O}$ were characterized by magnetic and Mössbauer studies. Despite repeated attempts, $[\mathbf{2}]\cdot\mathbf{4H_2O}$ could not be isolated cleanly enough for magnetic and Mössbauer studies.

As noted, the only exception to the above was complex **5**. In this case further synthetic modification was required as the addition of excess $NaCF_3SO_3$ to **1** in water did not give a precipitate. Hence IPA was added (to give a 1:1 water/IPA mixture), and refrigeration of this solution gave a relatively large sample (50 mg) of colorless single crystals of $[\mathbf{5}]\cdot{}^3/_4\mathbf{IPA}\cdot\mathbf{H_2O}$. This compound could not be recrystallized by the above method (dissolving in 4:1 MeCN/DMF followed by diffusion of diethylether vapor) as this gave only an oily brown material. Hence, the colorless crystals obtained from cooling of the water/IPA reaction solution were air-dried, giving $[\mathbf{5}]\cdot\mathbf{H_2O}$. This sample was used for magnetic and Mössbauer studies.

It is important to note that the solvation observed in the single crystals, $[\mathbf{2}]\cdot\mathbf{2MeOH}\cdot\mathbf{H_2O}$, $[\mathbf{5}]\cdot{}^3/_4\mathbf{IPA}\cdot\mathbf{H_2O}$, and $[\mathbf{7}]\cdot\mathbf{1.6MeOH}\cdot\mathbf{0.4H_2O}$, on which X-ray crystal structure determinations have been carried out (see below) in no case matches that of the bulk, air-dried, samples subsequently used for magnetic and Mössbauer studies ($[\mathbf{2}]\cdot\mathbf{4H_2O}$, $[\mathbf{5}]\cdot\mathbf{H_2O}$, and $[\mathbf{7}]\cdot\mathbf{2H_2O}$). As a consequence, differing spin states are observed by crystallography to those observed by the magnetic and Mössbauer studies (see below).

Generally the complexes were not air sensitive so were prepared without precautions to exclude air. The exception to this was complex **7**, which was air sensitive. For this, all manipulations, including recrystallization, were thus performed under an inert atmosphere of argon or nitrogen, and the reaction and recrystallization solvents were thoroughly degassed.

Structure of $[Fe_2(PMAT)_2]Cl_4\cdot2MeOH\cdot H_2O$. A small number of crystals of $[\mathbf{2}]\cdot\mathbf{2MeOH}\cdot\mathbf{H_2O}$, insufficient for magnetic studies but suitable for X-ray diffraction studies, were grown as orange blocks by Et_2O vapor diffusion into a MeOH solution of the complex. Two full X-ray data sets, the first at 90 K and the

dx.doi.org/10.1021/ic200308k |*Inorg. Chem.* 2011, 50, 4586–4597

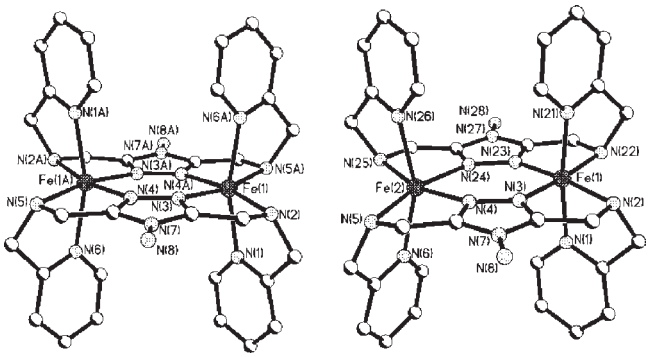

Figure 1. Perspective view of $[Fe_2(\mathbf{PMAT})_2]Cl_4\cdot 2MeOH\cdot H_2O$ ($[\mathbf{2}]\cdot\mathbf{2MeOH\cdot H_2O}$) at 293 K (LHS) and at 90 K (RHS). Anions, hydrogen atoms, and solvent molecules have been omitted for clarity.

second at 293 K, were collected. At both temperatures the space group is triclinic $P\bar{1}$. At 90 K the asymmetric unit contains one dinuclear complex, with four chloride anions, two methanol molecules, and one water of solvation, whereas at 293 K it comprises half of this.

At both temperatures (Figure 1), the iron centers are in an N_6 distorted octahedral environment, with three donors coming from each of two **PMAT** ligands, which sandwich the metal centers, in the same manner as seen in previously structurally characterized **PMAT** and related pyrazolate $\mathbf{PMAP}^-$ ($\mathbf{PMAP}^-$ is 3,5-bis{[*N*-(2-pyridylmethyl)amino]methyl}-1*H*-pyrazolate) complexes.[10−13,16]

At 90 K, Fe(1) has bond lengths ranging from 1.911(5) to 2.068(5) Å (Table 1) and *cis* N−Fe−N angles ranging from 81.3(2) to 102.1(2)°. These short bonds, and the close-to-octahedral geometry, are typical of LS iron(II). In contrast, Fe(2) has longer bonds [2.120(5) to 2.299(5) Å], and a more distorted geometry [*cis* N−Fe−N angles range from 76.6(2) to 120.1(2)°], consistent with Fe(2) being in the HS state. Hence, this is just the second example of a structure determination clearly revealing mixed spin states *within* a dimetallic complex (the first was **1**). As expected, the details of the iron(II) geometries in $[\mathbf{2}]\cdot\mathbf{2MeOH\cdot H_2O}$ are similar to those observed for **1** at 123 K (Table 1).

In total, at 90 K, the structure is stabilized by 14 hydrogen bonds (Figure 2, Supporting Information, Table S1) which vary considerably in strength, (D···A ranges from 3.059(5) to 3.517(5) Å). These include amino, methanolic, and aqueous proton to chloride interactions. The hydrogen bonds between the chloride counterions and amino protons cause the complexes to line up such that planar sections of the ligand are parallel to those in adjacent complexes, forming an ordered 2D array (Figure 3).

For the room-temperature data collection the asymmetric unit contains one-half of the dinuclear complex, one full-occupancy MeOH, and one-half-occupancy water, with the other half of the complex generated by a center of inversion between the two iron centers (Figure 1).

The iron center remains in an N_6 distorted octahedral environment, with three donors coming from each of two **PMAT** ligands. The Fe−N distances range from 2.072(7) to 2.275(7) Å (Table 1), and the *cis* N−Fe−N angles from 76.0(3) to 116.0(3)°. These bond lengths and angles are very similar to those observed for the HS center in the low-temperature structure, and even more so to **1** in the [HS-HS] state, and are typical of HS iron(II).

The room-temperature structure is stabilized by eight intermolecular hydrogen-bonds (Supporting Information, Figure S1, Table S2). Despite this reduction in the extent of the hydrogen bonding a very similar overall packing arrangement (Supporting Information, Figure S2) is obtained to that observed for the low-temperature structure (Figure 3).

Structure of $[Fe_2(PMAT)_2](CF_3SO_3)_4\cdot{}^3/_4IPA\cdot H_2O$. A large number of block shaped crystals of $[\mathbf{5}]\cdot{}^3/_4\mathbf{IPA\cdot H_2O}$ were grown by cooling the IPA/H_2O reaction solution in a refrigerator for 3 days. The complex crystallizes in the monoclinic space group $P2_1/c$ and the asymmetric unit comprises two halves of two crystallographically independent complex molecules (Figure 4 and Supporting Information, Figure S3). A center of inversion generates the other half of both molecules. The complex also crystallizes with 3/4 of an interstitial isopropanol and one interstitial water molecule. Just as in the previous $[Fe_2(\mathbf{PMAT})_2]X_4$ complexes, both of the iron(II) centers have N_6 coordination spheres with all six nitrogen donor atoms coming from the two **PMAT** ligands. The bond lengths and angles observed for the iron centers in $[\mathbf{5}]\cdot{}^3/_4\mathbf{IPA\cdot H_2O}$ at 90 K (Table 1) are consistent with those expected for iron(II) in the HS state.

The two crystallographically independent complexes present in $[\mathbf{5}]\cdot{}^3/_4\mathbf{IPA\cdot H_2O}$ differ mainly in the way that they interact with the counteranions and interstitial solvent molecules through anion···π and N−H···O hydrogen bonding interactions (Figure 4, Supporting Information, Figures S4 and S5; Table S3). In the Fe(1) complex there are two quite strong anion···π interactions between the triflates and one triazole ring [O(71)···centroid =3.003 Å and F(43)···centroid = 2.995 Å; Figure 4], forming an anion···π···anion sandwich similar to those reported by us previously.[17] In the Fe(2) complex there is only one anion···π interaction to the triazole ring [O(41)···centroid = 3.273 Å], with the "other" side of the ring blocked by the partial occupancy IPA molecule (Figure 4).

The triflate counteranions and the interstitial solvent molecules in $[\mathbf{5}]\cdot{}^3/_4\mathbf{IPA\cdot H_2O}$ form many hydrogen bonds to the N−H protons of the two complexes, similar to the situation observed for $[\mathbf{2}]\cdot\mathbf{2MeOH\cdot H_2O}$ (Figure 2). The complex containing Fe(1) only has N−H···anion hydrogen bonds, while the complex containing Fe(2) has interactions not only to the anion oxygen atoms, but also to the interstitial solvent molecules. [Supporting Information, Figures S4 and S5; N···O = 2.68-(3)−3.204(10) Å and <(N−H···O) = 116.0−165.4; Supporting Information, Table S3).

Structure of $[Fe_2(PMAT)_2](C_{16}SO_3)_4\cdot 1.6MeOH\cdot 0.4H_2O$. A few single crystals of $[\mathbf{7}]\cdot\mathbf{1.6MeOH\cdot 0.4H_2O}$ were obtained as triangular pale orange plates by the vapor diffusion of diethyl ether into a methanolic solution of $[Fe_2(\mathbf{PMAT})_2](C_{16}SO_3)_4$, and the X-ray structure was determined at 90 K (Figure 5, Supporting Information, Figures S6−S8). The insoluble nature of the complex in acetonitrile (even in 4:1 DMF/MeCN) and the slight solubility in methanol led us to use this method to obtain the crystals. Complex $[\mathbf{7}]\cdot\mathbf{1.6MeOH\cdot 0.4H_2O}$ crystallizes in the triclinic space group $P\bar{1}$ with half of the dinuclear complex in the asymmetric unit. The other half of the complex is generated by a center of inversion (Supporting Information, Figure S6).

The iron(II) center has a distorted N_6 coordination sphere (Table 1) with Fe−N bond lengths [2.022(5)−2.137(5) Å] and *cis* N−Fe−N angles [79.0(2)−111.2(2)°] that are consistent with HS iron(II). The primary and secondary amine protons form hydrogen-bonding interactions to the oxygen atoms of the

dx.doi.org/10.1021/ic200308k |*Inorg. Chem.* 2011, 50, 4586–4597

Table 1. Comparison of Selected Bond Distance [Å] and Angle [deg] Ranges, and Selected Other Data, for $[Fe_2(PMAT)_2](BF_4)_4 \cdot DMF$ (1·DMF), $[Fe_2(PMAT)_2]Cl_4 \cdot 2MeOH \cdot H_2O$ ([2]·2MeOH·H_2O), $[Fe_2(PMAT)_2](CF_3SO_3)_4 \cdot {}^3/_4IPA \cdot H_2O$ ([5]·$^3/_4$IPA·H_2O), $[Fe_2(PMAT)_2](C_{16}SO_3)_4 \cdot 1.6MeOH \cdot 0.4H_2O$ ([7]·1.6MeOH·0.4H_2O)

	1·DMF[10]		[2]·2MeOH·H_2O		[5]·$^3/_4$IPA·H_2O	[7]·1.6MeOH·0.4H_2O
	X = BF_4		X = Cl		X = CF_3SO_3	X = $C_{16}H_{33}SO_3$
	123 K	298 K	90 K	293 K	91 K	90 K
	[HS-LS]	[HS-HS]	[HS-LS]	[HS-HS]	[HS-HS]	[HS-HS]
Fe−N_{pyr} [Å]	Fe(HS) 2.159(4), 2.155(4) Fe(LS) 1.934(3), 1.986(4)	2.148(),2.147(5)	Fe(HS) 2.145(5), 2.155(5) Fe(LS) 1.980(5), 1.982(5)	2.107(8), 2.136(7)	Fe(1) 2.081(7), 2.069(9) Fe(2) 2.104(7), 2.083(6)	2.055(6), 2.0756)
Fe−N_{NH} [Å]	Fe(HS) 2.319(4), 2.312(4) Fe(LS) 2.066(4), 2.071(4)	2.289(5), 2.303(5)	Fe(HS) 2.299(5), 2.245(5) Fe(LS) 2.057(5), 2.068(5)	2.242(6), 2.275(7)	Fe(1) 2.245(10), 2.218(7) Fe(2) 2.227(7), 2.255(9)	2.137(5), 2.123(5)
Fe−N_{triaz} [Å]	Fe(HS) 2.136(3), 2.131(3) Fe(LS) 1.946(3), 1.934(3)	2.123(4), 2.116(4)	Fe(HS) 2.120(5), 2.121(5) Fe(LS) 1.911(5), 1.916(5)	2.072(7), 2.095(6)	Fe(1) 2.026(9), 2.075(7) Fe(2) 2.045(7), 2.077(8)	2.022(5), 2.025(5)
average Fe−N [Å]	Fe(HS) 2.202 Fe(LS) 1.989	2.188	Fe(HS) 2.181 Fe(LS) 1.986	2.155	Fe(1) 2.119 Fe(2) 2.132	2.073
cis-N−Fe−N [deg] range	Fe(HS) 75.1(2)−121.7(2) Fe(LS) 81.8(2)−101.1(2)	75.9(2)−115.9(2)	Fe(HS) 76.6(2)−120.1(2) Fe(LS) 81.3(2)−102.1(2)	76.0(3)−116.0(3)	Fe(1) 76.7(4)−114.3(4) Fe(2) 76.8(3)−114.9(3)	79.0(2)−111.2(2)
trans-N−Fe−N [deg] range	Fe(HS) 154.2(2)−163.2(2) Fe(LS) 170.9(2)−175.9(2)	161.3(2)−167.7(2)	Fe(HS) 157.7(2)−163.1(2) Fe(LS) 172.2(2)−175.2(2)	163.3(3)−166.8(3)	Fe(1) 159.0(3)−168.7(2) Fe(2) 159.2(3)−167.6(3)	165.0(2)−169.8(2)
average *cis*-N−Fe−N [deg]	Fe(HS) 91.0 Fe(LS) 90.1	90.5	Fe(HS) 90.9 Fe(LS) 90.1	90.5	Fe(1) 90.5 Fe(2) 90.6	90.4
average *trans*-N−Fe−N [deg]	Fe(HS) 160.0 Fe(LS) 173.1	165.1	Fe(HS) 161.0 Fe(LS) 174.2	165.6	Fe(1) 165.2 Fe(2) 164.7	167.9
Σ [deg] [a]	Fe(HS) 133.1 Fe(LS) 64.9	117.5	Fe(HS) 123.1 Fe(LS) 69.7	110.4	Fe(1) 109.6 Fe(2) 109.5	87.5

[a] Distortion parameter Σ (defined as the sum of the absolute values of the deviation from 90° of the 12 *cis* angles in the coordination sphere).[18b]

dx.doi.org/10.1021/ic200308k |*Inorg. Chem.* 2011, 50, 4586–4597

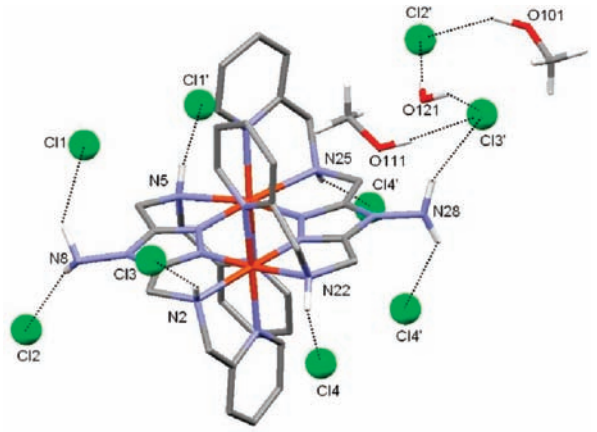

Figure 2. Perspective view of the hydrogen bonding in $[Fe_2(\mathbf{PMAT})_2]Cl_4 \cdot 2MeOH \cdot H_2O$ ($[\mathbf{2}] \cdot \mathbf{2MeOH \cdot H_2O}$) at 90 K. Hydrogen atoms, other than the N−H, O−H and methyl hydrogen atoms, have been omitted for clarity.

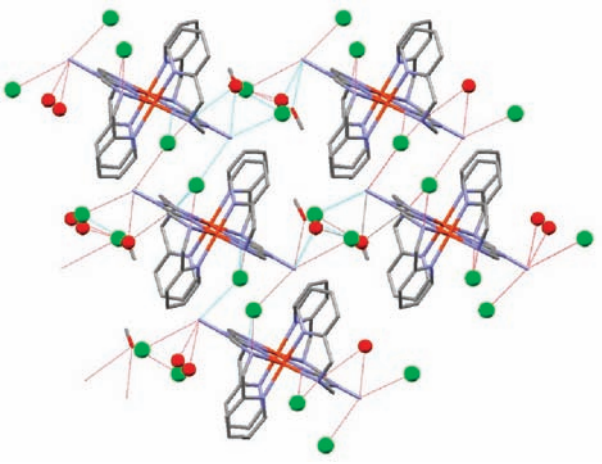

Figure 3. Perspective view of the packing of $[\mathbf{2}] \cdot \mathbf{2MeOH \cdot H_2O}$ at 90 K. Large green balls represent chloride counteranions and red balls are interstitial solvent molecules. Hydrogen atoms have been omitted for clarity.

sulfonate based counteranions [N−H···O = 2.877(7)−3.358(9) Å and <N−H···O = 124.7−166.8°; Supporting Information, Figures S7 and S8; Table S4].

The packing in this complex involves layers of cations separated by layers of counteranions, with the long alkyl chains of the anions interdigitating, resulting in a large separation between cationic components (~31 Å, Figure 5). The anions interact with the cations not only through the aforementioned hydrogen bonding interactions, but also through a relatively strong anion ···π interaction between a triazole ring and a sulfonate oxygen atom [O(11)···centroid = 2.898 Å, Supporting Information, Figure S8].

Structural Comparisons. With the ligand remaining constant across the four crystallographically characterized complexes it is unsurprising that the iron(II) geometries are generally very similar. In all cases, two **PMAT** ligands provide all 12 nitrogen donor atoms to the two six-coordinate iron(II) centers. However, clearly these structures do differ in spin state, as some are [HS-HS] while others are [HS-LS]. Despite this, it is interesting

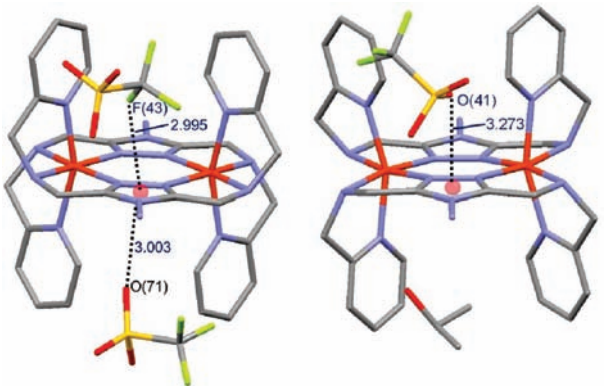

Figure 4. Perspective views of the two different anion-π interactions in $[Fe_2(\mathbf{PMAT})_2](CF_3SO_3)_4 \cdot {}^3/_4IPA \cdot H_2O$ ($[\mathbf{5}] \cdot {}^3/_4\mathbf{IPA \cdot H_2O}$) at 90 K. Hydrogen atoms, solvent molecules, and remaining counteranion have been omitted for clarity. LHS: anion-π-anion sandwich interaction in one of the two independent complexes, Fe(1). RHS: anion-π interaction and the blocking of the "other" face of the triazole ring by the partial occupancy interstitial IPA molecule in the second of the two independent complexes, Fe(2).

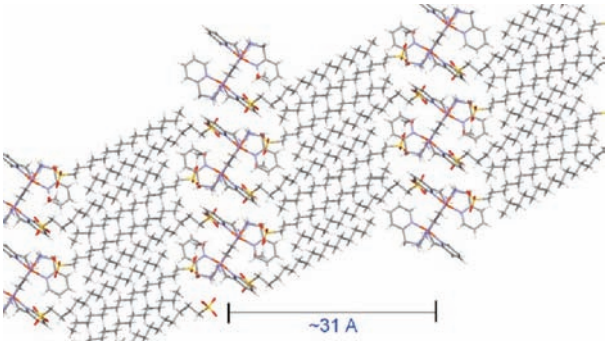

Figure 5. Perspective view of packing in $[Fe_2(\mathbf{PMAT})_2](C_{16}SO_3)_4 \cdot 1.6MeOH \cdot 0.4H_2O$ ($[\mathbf{7}] \cdot \mathbf{1.6MeOH \cdot 0.4H_2O}$), highlighting the distance between stacks of cationic species.

to note that the average *cis*-N−Fe−N angle falls within a remarkably narrow range, 90.1 and 91.0°, and the average *trans*-N−Fe−N angle falls between 160.0 and 174.2° (Table 1), so clearly it is important to look more closely than this to identify the key differences between these structures.

The Fe−N bond distances fall in distinctive ranges: 1.986−1.989 Å for LS in [HS-LS]; 2.181−2.202 Å for HS in [HS-LS] and 2.073/2.155−2.188 Å for HS in [HS-HS]. Likewise the *cis*-N−Fe−N angles fall in characteristic ranges: 81.3−102.1° for LS in [HS-LS]; 75.1−121.7° for HS in [HS-LS] and 75.9−116.0° for HS in [HS-HS]. That is, as expected, HS iron(II) results in significantly longer bond lengths and more widely ranging angles. However, in this case it is also possible to observe the effect of all 12 donors to the two six-coordinate iron(II) centers coming from just two hexadentate **PMAT** ligands, as the HS centers in the mixed [HS-LS] structures are somewhat more distorted than in the fully [HS-HS] structures (see also distortion parameter,[18b] Σ, Table1). This presumably reflects the impact of the two ligands adopting shorter bonds and closer to octahedral angles at the LS center, leading to greater distortions at the more accommodating HS center. This also disfavors *both* centers going LS; [LS-LS] is not seen.

dx.doi.org/10.1021/ic200308k |*Inorg. Chem.* 2011, 50, 4586–4597

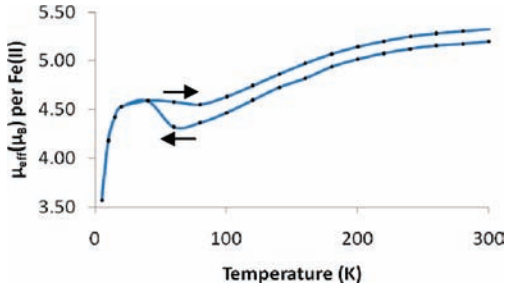

Figure 6. Plot of effective magnetic moment per iron(II) vs temperature for the bromide complex [**4**]·**2H$_2$O**. Solid line simply joins the data points (black dots) to aid the eye. Cooling mode is the lower curve. Heating mode is the higher curve; subsequent cooling and heating of this sample gave the same curve as the heating mode (higher curve).

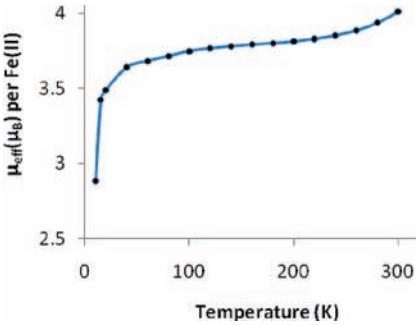

Figure 7. Plot of μ_{eff} (μ_B) per iron(II) vs temperature (K) for the $C_{16}H_{33}SO_3$ complex [**7**]·**2H$_2$O**. Black dots are data points; solid line simply joins the data points to aid the eye.

Other than for the HS iron(II) center in the $C_{16}SO_3$ complex, [**7**]·**1.6MeOH**·**0.4H$_2$O**, which has a distortion parameter of just 87.5°, the distortion parameter for the HS iron(II) centers is greater than 109°. In contrast, all of the LS iron(II) centers feature a distortion parameter of less than 70° (Table 1). Not surprisingly, given the highly constrained nature of the binding of the bis-tetradentate **PMAT** ligand, these values are higher than the distortions observed for the iron(II) center in ten [$Fe^{II}L_2(NCS)_2$] complexes of far simpler bidentate ligand systems, that have been structurally characterized in both HS and LS states (average Σ(HS) = 80(5)°, average Σ(LS) = 47(5)°].[19] Closer analysis of the distortion parameters in the [HS-HS] versus [HS-LS] forms of both [**1**]·**DMF** and [**2**]·**2MeOH**·**H$_2$O** also reveals that in both cases the HS center in the [HS-LS] mixed spin state structures is significantly more distorted (133.1° and 123.1°, respectively) than in the [HS-HS] structures (117.5° and 110.4°, respectively).

Magnetochemistry Studies. Magnetic measurements were carried out from 300−5 K on solid samples of five of the six new complexes (Supporting Information, Figures S9−S13): a clean "bulk" sample of the chloride complex **2** could not be isolated despite repeated attempts, so it was not studied. All complexes displayed a temperature mediated SCO event on cooling from 300 K.

The PF_6 complex, **3**, is the only solvent-free sample studied (Supporting Information, Figure S9). It remains mainly (see Mössbauer section, later) in the [HS-HS] configuration from 300 to 200 K (μ_{eff} = 5.00 μ_B per iron), from which point the effective magnetic moment gradually decreases over 120 K before reaching a plateau at $\mu_{eff} \approx 4.4\ \mu_B$ per iron from 80−50 K (after this zero-field splitting (ZFS) causes a large decrease in μ_{eff}). The value of μ_{eff} in the plateau region is significantly higher than the $\mu_{eff} \approx 3.88\ \mu_B$ per iron observed for the [HS-LS] form of [**1**]·**DMF**,[10−12] most likely because of only a partial conversion to the [HS-LS] species in the case of **3**, that is, there is the possibility of there being more than one unique [HS-HS] species in the sample; thus, an approximate 1:1 ratio of [HS-LS] to [HS-HS] would give the observed μ_{eff}.

The SbF_6 complex, [**4**]·**2H$_2$O**, has a similar magnetic profile; however, the decrease in μ_{eff} begins at a higher temperature (260 K, Figure 6). The effective moment decreases from 5.29 μ_B per iron at 300 K, consistent with a [HS-HS] state, to 4.32 μ_B per iron at 60 K, before suddenly rising to 4.59 μ_B per iron at 40 K (Figure 6, cooling mode is the lower curve). From 35 K and below ZFS causes the decrease in μ_{eff}. Intriguingly, when the sample was then warmed back up from 5 to 300 K the profile starts off following the same path as the cooling mode; however, at 40 K the magnetic moments are no longer the same and the μ_{eff} now follows a small plateau from 40−80 K with μ_{eff} = 4.6 μ_B per iron (Figure 6). From 80−300 K the μ_{eff} very gradually rises to 5.42 μ_B per iron; however, it never follows exactly the same path as the cooling mode. These results suggest that an irreversible phase change has occurred on cooling. Subsequent heating and cooling measurements on the same sample confirm that the phase change was irreversible as all of these runs follow the original heating (not cooling) profile (Figure 6). The small plateau from 40−80 K with μ_{eff} = 4.6 μ_B per iron is consistent with the presence of approximately a 1:1 ratio of [HS-LS] to [HS-HS] (similarly, Mössbauer spectroscopy at 4.6 K indicates a ratio of 75:25 HS/LS, see below).

The trifluoromethanesulfonate complex [**5**]·**H$_2$O** also displays a gradual temperature mediated SCO event, between 220−150 K, with $T_{1/2}$ = 180 K (Supporting Information, Figure S11). In this complex the plateau region, with $\mu_{eff} \sim 4.0\ \mu_B$ per iron, is consistent with an approximate 58:42 HS/LS ratio (NB. the range is large, ± 7; Supporting Information, Table S5; Figure S14), that is, mainly [HS-LS] with only a trace of the [HS-HS] contamination seen for the previous two complexes (X = PF_6 and SbF_6). Interestingly, and in contrast to the magnetic data on the PF_6 and SbF_6 complexes, the triflate complex is not fully [HS-HS] at room temperature. Rather it appears to be approximately a 1:2 ratio of [HS-LS] to [HS-HS] (μ_{eff} = 4.8 μ_B per iron). The low-temperature structure determination on [**5**]·$^3/_4$**IPA**·**H$_2$O** (note the different solvent content of the single crystals) reveals that the iron(II) centers are all in the HS configuration at 89 K. This is in contrast to the magnetic and Mössbauer data on [**5**]·**H$_2$O** which both indicate that at 89 K the sample contains both HS and LS iron(II). This is most likely because of the different solvation of the complex in the single crystals used for the structure determination versus the powder sample used for the magnetic and Mössbauer studies as solvent is known to be important,[8,20] that is, the presence of IPA and H_2O in the crystal lattice prevents SCO from occurring at or above 89 K, whereas in the powder, the presence of the water molecule and/or absence of the IPA presumably facilitates this, as SCO occurs at 180 K.

The tetrakis(4-fluorophenyl)borate complex, [**6**]·$^1/_2$**MeCN**, displays a very gradual SCO that begins well above 300 K (Supporting Information, Figure S12). At 300 K the effective magnetic moment is 4.22 μ_B, consistent with the system having approximately 64:36 HS/LS (NB. the range is large, ± 7, Supporting Information, Table S5; Figure S14), that is, it is part way through the SCO transition. At 75 K the effective magnetic

dx.doi.org/10.1021/ic200308k |*Inorg. Chem.* 2011, 50, 4586–4597

Table 2. Temperature Dependent ^{57}Fe Mössbauer Parameters of Complexes [3], [4]·2H$_2$O, [5]·H$_2$O, [6]·$^1/_2$MeCN, and [7]·2H$_2$O

sample	T (K)	species	δ (mm s^{-1})	ΔE_Q (mm s^{-1})	Γ_L (mm s^{-1})	Γ_R (mm s^{-1})	I (%)
3 (PF_6^-)	4.6	HS "1"	1.16	3.39	0.51	0.51	20
		HS "2"	1.08	2.85	0.39	0.39	37
		LS	0.49	0.22	0.27	0.27	43
	296	HS "1"	1.06	2.95	0.51	0.51	24
		HS "2"	0.95	2.35	0.39	0.39	44
		LS	0.39	0	0.50	0.50	32
[**4**]·**2H$_2$O** (SbF_6^-)	4.6	HS	1.08	2.83	0.34	0.34	73
		LS	0.5	0.28	0.24	0.24	27
	296	HS	0.96	2.49	0.28	0.28	80
		LS[a]	0.45	0.49	0.30	0.30	20
[**5**]·**H$_2$O** ($CF_3SO_3^-$)	4.6	HS	1.09	2.83	0.32	0.32	50
		LS	0.50	0.25	0.29	0.29	50
	296	HS	0.95	2.46	0.29	0.33	75
		LS	0.31	0	0.55	0.55	25
[**6**]·**1/2MeCN** ($B(PhF)_4^-$)	4.6	HS	1.10	2.85	0.46	0.49	60
		LS	0.49	0.26	0.33	0.33	40
	296	HS	0.97	2.40	0.46	0.49	60
		LS	0.34	0.34	0.26	0.55	40
[**7**]·**2H$_2$O** ($C_{16}H_{33}SO_3^-$)	4.6	HS	1.06	2.54	0.48	0.48	50
		LS	0.48	0.20	0.30	0.30	50
	296	HS	0.92	1.96	0.48	0.48	38
		LS	0.38	0	0.40	0.40	62

[a] The % effect is so low that these parameters are only approximate.

Table 3. Comparison of the Spin State Information Obtained from Magnetic and Mössbauer Studies, at Low and Room Temperature, on Complexes [3], [4]·2H$_2$O, [5]·H$_2$O, [6]·$^1/_2$MeCN, and [7]·2H$_2$O[a]

		approximate HS/LS ratios			
complex	anion	4.6 K (Mössbauer)[b]	50 K (magnetic)[c]	296 K (Mössbauer)[b]	300 K (magnetic)[c]
[**3**]	PF_6	57:43 ± 2	(4.40) 70:30	68:32 ± 3	(5.00) 90:10
[**4**]·**2H$_2$O**	SbF_6	73:27 ± 3	(4.32) 67:33[d] cooling	80:20[e] ± 6	(5.29) 100:0
			(4.60) 78:22 warming		
[**5**]·**H$_2$O**	CF_3SO_3	50:50 ± 2	(4.0) 58:42	75:25 ± 5	(4.80) 83:17 cooling
[**6**]·**$^1/_2$MeCN**	$B(PhF)_4$	60:40 ± 3	(3.73) 50:50	60:40 ± 5	(4.22) 64:36
[**7**]·**2H$_2$O**	$C_{16}H_{33}SO_3$	50:50 ± 2	(3.80) 52:48	40:60[f] ± 5	(4.00) 58:42

[a] Errors in the HS/LS ratio from Mössbauer studies are provided through careful curve-fitting. For magnetic studies both the approximate ratio of HS/LS (note that the range either side of this value is large, approx. ±11; see Supporting Information, Table S5 and Figure S14) and the μ_{eff} value per iron(II) used to estimate this are provided. Note (a) because of ZFS effects the low temperature values for the magnetic data were obtained from the data at 50 K (whereas the low temperature Mössbauer spectra were run at 4.6 K) and (b) the different solvent content of these samples versus the single crystals used in the X-ray structural analyses is the likely cause of differences between the values in this table and those observed crystallographically. [b] Approximate HS/LS ratio as obtained from fitting the Mössbauer data. [c] Approximate HS/LS ratio calculated from the magnetic data as follows (note that the range either side of this value is large, approximately ±11;see Supporting Information for more details). The accepted range of μ_{eff} per HS iron(II) is 5.0−5.6 μ_B. Hence 5.0 and 5.6 μ_B were each converted to χT values per iron, then to χT values for a [HS-HS] dimer and for a [LS-HS] dimer (half the previous value). This allowed two lines to be drawn on a plot of %HS vs χT per iron (see Supporting Information, Figure S14), one line for each μ_{eff} value (5.0 and 5.6 μ_B), by connecting the two extreme points, at 100% HS ≡ [HS-HS] and 50% HS ≡ [LS-HS] in each case. The approximate ratio given in the table (note range is approximately ±11) of HS/LS for these dinuclear iron(II) complexes was estimated using these two lines. To do so the observed μ_{eff} of interest was converted to χT and the two possible %HS obtained from the two lines; the value shown in this table is the average of these two numbers (see also Supporting Information, Table S5). [d] At 60 K, as no data point at 50 K. [e] This ratio is difficult to determine because of the low % effect and signal-to-noise ratio. [f] An unlikely change, exhibited by more than one sample preparation that can instead be explained as a texture effect caused by the long alkyl chain of the anion.

moment plateaus at 3.7 μ_B, consistent with the [HS-LS] configuration. Below 25 K the rapid drop in the effective magnetic moment is caused by ZFS effects.

The $C_{16}SO_3$ complex, [**7**]·**2H$_2$O**, shows another temperature-mediated switch from [HS-HS] to [HS-LS]. In this complex the $T_{1/2}$ is again above 300 K (Figure 7). At 300 K the effective

dx.doi.org/10.1021/ic200308k |Inorg. Chem. 2011, 50, 4586–4597

moment is 4.0 μ_B per iron (approximately 58:42 HS/LS) and until 200 K the moment decreases gradually. From 200−50 K the effective moment remains at ∼3.8 μ_B per iron, consistent with a [HS-LS] configuration. This is the highest temperature observed for SCO in this family of dinuclear complexes. As for the triflate complex, $[5]\cdot\mathbf{H_2O}$, the data from the structure determination and the magnetic measurements do not agree with regard to the spin state present at 90 K. Again this is put down to the differences in solvation of the single crystal ($[7]\cdot\mathbf{1.6MeOH}\cdot\mathbf{0.4H_2O}$) versus the powder sample ($[7]\cdot\mathbf{2H_2O}$).

Complex $[7]\cdot\mathbf{2H_2O}$ not only features a promising, close to room temperature SCO event; it also represents our first step toward new types of *dinuclear* SCO compounds, specifically those in which a long alkyl chain is present (in this case from the hexadecyl sulfonate anions[15]). This opens up the possibility of forming Langmuir−Blodgett (LB) films of the complexes at a surface.[15,21] This in turn is important as such assembly/ordering of the complexes at an interface can (a) cause a gradual SCO event to become more abrupt because of many-body interactions, (b) remove the complex effects of crystal packing and morphology on SCO, and (c) open up the possibility of starting to address the attachment/layering of functional molecules onto a solid support. While taking such studies to this next, multidisciplinary stage is very challenging, it is important that we start to address these points, in particular the last one, as they are important for future applications. However, in this case complex $[7]\cdot\mathbf{2H_2O}$ does not form stable films. There are two likely causes for this failure: (a) the use of a tailed anion, while synthetically elegant, is not always as effective at inducing film formation as having the tail covalently attached to the ligand which binds directly the iron(II),[15,21] and/or (b) the **PMAT** ligand itself is not sufficiently robust in solution with iron(II) in air. One of our current aims is therefore to generate more chemically robust, tailed, versions of ligands such as **PMAT**.

Mössbauer Studies. ^{57}Fe Mössbauer studies reveal important information concerning the iron centers and how the anion variation influences them. Initial inspection of the data suggests that, as one would expect with a family of compounds, the Mössbauer parameters are remarkably similar (Table 2). The isomer shift and quadrupole splittings for HS iron(II) at 4.6 K are all aproximately 1.1 and 2.9 mm s^{-1}, respectively. Likewise, all of the LS iron(II) show similar isomer shifts and quadrupole splittings, of 0.5 and 0.2 mm s^{-1}, respectively, at 4.6 K. As the temperature is raised to 296 K the isomer shifts for HS and LS iron(II) all decrease by approximately 0.13 mm s^{-1}, consistent with the second-order Doppler shift.[22] In general the HS iron(II) in all of these complexes shows a decrease in the quadrupole splitting of 0.4 mm s^{-1}, as is commonly observed.[23]

As expected, the main differences in the Mössbauer spectra of this series of complexes result from the different SCO properties. Fitting of the data with pairs of quadrupole doublets with Lorentzian line shape allows the ratios of HS/LS at each temperature to be determined, and these are in broad agreement with the magnetic data (Table 3).

The complexes with the very large anions, $[6]\cdot{}^1/_2\mathbf{MeCN}$ ($B(PhF)_4^-$) and $[7]\cdot\mathbf{2H_2O}$ ($C_{16}H_{33}SO_3^-$), exhibit only a hint of SCO (beginning at the high end of the temperature range examined), and unlike all of the other complexes these two never attain more than 60:40 HS/LS.

The Mössbauer spectra of $[6]\cdot{}^1/_2\mathbf{MeCN}$ indicate that it remains 60:40 HS/LS over all temperatures (Figure 8), whereas the magnetic measurements suggest that there may be a very gradual SCO to 50:50 HS/LS at 50 K (Table 3). However, it should be noted that the range for the latter ratio is large, ± 6 (see Supporting Information, Table S5 and Figure S14).

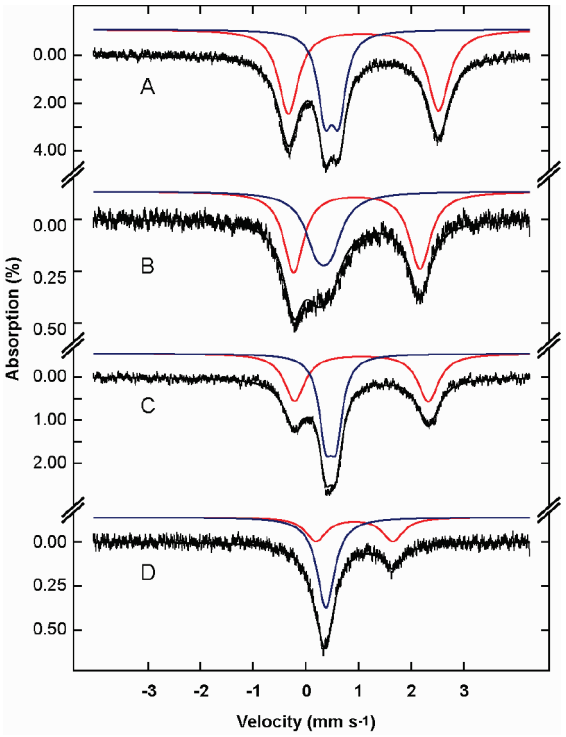

Figure 8. Variable temperature Mössbauer spectra of $[6]\cdot{}^1/_2\mathbf{MeCN}$ ($B(PH_4)^-$) and $[7]\cdot\mathbf{2H_2O}$ ($C_{16}H_{33}SO_3^-$). All spectra consist of two quadrupole doublets corresponding to HS (red line) and LS (blue line) Fe(II). $[6]\cdot{}^1/_2\mathbf{MeCN}$ exists in a 60:40 HS/LS ratio at both 4.6 K (A) and 296 K (B). $[7]\cdot\mathbf{2H_2O}$ exists in a 50:50 HS/LS ratio at 4.6 K (C), while at 296 K (D) this ratio changes to approximately 40:60 HS/LS. This nonsensical change, exhibited by more than one sample preparation, can be explained as a texture effect caused by the long alkyl chain of the anion.

Consistent with the magnetic data, complex $[7]\cdot\mathbf{2H_2O}$ is 50:50 HS/LS at 4.6 K. However, it shows what appears to be a decrease in the amount of HS at higher temperatures, which cannot be true (Figure 8). Rather than an inverse spin transition, it indicates a decrease in the Lamb−Mössbauer factor, which has been observed in more than one preparation of this sample. It may be due to a texture effect[22] and, indeed, similar effects have been observed in related long-chain-substituted complexes.[21]

Complexes with the intermediate sized anions **3** (PF_6^-), $[4]\cdot\mathbf{2H_2O}$ (SbF_6^-), and $[5]\cdot\mathbf{H_2O}$ ($CF_3SO_3^-$) all show SCO, although according to the Mössbauer data the spin transition never quite goes to completion, that is, to fully [HS-HS], over the temperature range 4.6 to 296 K (Figure 9). At 4.6 K, complex $[4]\cdot\mathbf{2H_2O}$ exists as 75:25 HS/LS, **3** exists as 60:40 HS/LS, while $[5]\cdot\mathbf{H_2O}$ exists in a 50:50 HS/LS state. At 296 K, the amount of HS iron(II) present in all three complexes has increased somewhat: complex $[4]\cdot\mathbf{2H_2O}$ is 80:20 HS/LS, **3** is 70:30 HS/LS, and $[5]\cdot\mathbf{H_2O}$ is 75:25 HS/LS. Please note, however, that the sample of $[4]\cdot\mathbf{2H_2O}$ used for Mössbauer investigations was small, leading to a low signal-to-noise ratio. The 80:20 HS/LS ratio determined at 296 K may well overestimate the amount of LS.

At both 4.6 and 296 K, complex **3** exhibits an asymmetric HS state (Figure 10), which can be modeled by two HS quadrupole doublets in a ratio of approximately 2:1 (Table 2). Putting all the

dx.doi.org/10.1021/ic200308k |*Inorg. Chem.* 2011, 50, 4586–4597

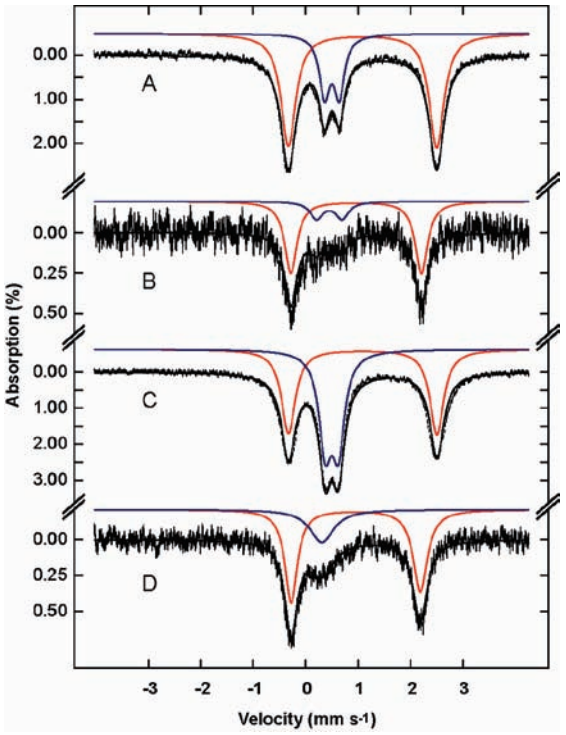

Figure 9. Variable temperature Mössbauer spectra of $[4]\cdot 2\mathbf{H_2O}$ (SbF_6^-) and $[5]\cdot \mathbf{H_2O}$ ($CF_3SO_3^-$). All spectra consist of two quadrupole doublets corresponding to HS (red line) and LS (blue line) Fe(II). $[4]\cdot 2\mathbf{H_2O}$ clearly shows a spin transition from 75:25 HS/LS at 4.6 K (A) to approximately 80:20 HS/LS at 296 K (B), although this ratio is difficult to determine because of the low % effect and signal-to-noise ratio (the magnetic data indicate a value closer to fully HS at 300 K). $[5]\cdot \mathbf{H_2O}$ shows a similar spin transition but starts from 50:50 HS/LS at 4.6 K (C) and changes to a 75:25 HS/LS ratio at 296 K (D).

Mössbauer data together suggests that all of these complexes switch as a "dimer of dimers", that is, each complex occupies a different part of the energy landscape from 2[HS-LS] (**3**, $[5]\cdot \mathbf{H_2O}$, $[7]\cdot 2\mathbf{H_2O}$) to [HS-HS] [HS-LS] ($[4]\cdot 2\mathbf{H_2O}$, $[6]\cdot {}^1/_2\mathbf{MeCN}$).

CONCLUSION

As expected the anion choice affects the magnetic properties of this family of dinuclear iron(II) complexes. The original complex $[1]\cdot \mathbf{DMF}$ displays an abrupt [HS-HS] to [HS-LS] SCO event at 224 K whereas the complexes presented in this paper have different SCO profiles. The majority of the $[Fe^{II}{}_2(\mathbf{PMAT})_2]X_4$ family are SCO active; however, each differs not only in the $T_{1/2}$ value but also in the completeness and abruptness of the SCO. Although the anion choice changes the SCO, the [LS-LS] form is not seen due to it being structurally (Σ) disfavoured in $[Fe^{II}{}_2(\mathbf{PMAT})_2]X_4$ complexes. Despite six of the new complexes being exposed to DMF, none were obtained as DMF solvates. To date, the original complex, which is a DMF solvate, $[1]\cdot \mathbf{DMF}$, has the most abrupt SCO observed in this family. The present complexes, where SCO occurs, all have gradual SCO events and in some cases they are incomplete. Of this family, complex $[7]\cdot 2\mathbf{H_2O}$ is probably the most interesting as it contains a long-tailed anion and exhibits a gradual SCO event with a $T_{1/2}$ value near, though above, room temperature, a likely requirement for future nanoswitches and memory devices.

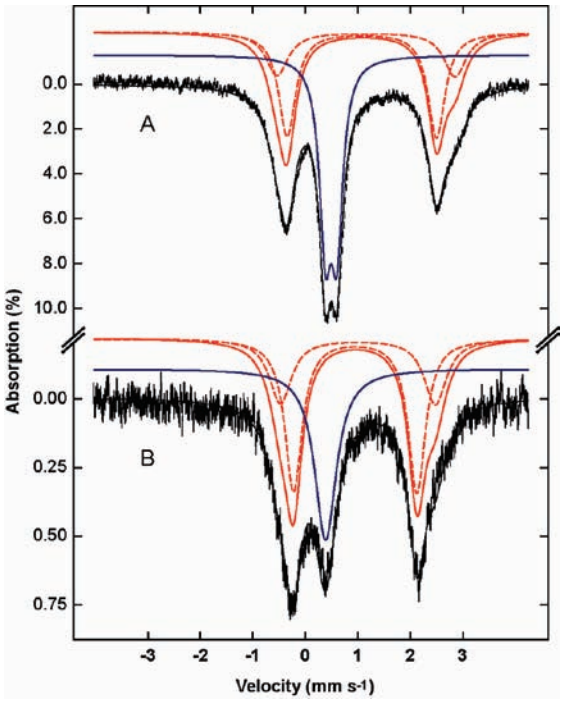

Figure 10. Variable temperature Mössbauer spectra of **3** (PF_6^-). Both spectra consist of two quadrupole doublets corresponding to HS (red line) and LS (blue line) Fe(II). The spectra show the presence of a spin transition from approximately 60:40 HS/LS at 4.6 K (A) to approximately 70:30 HS/LS at 296 K (B). The line shape of the quadrupole doublet caused by HS iron(II) in both spectra requires that it be fitted to two species in the ratio 1:2 (two sets of dotted red lines).

EXPERIMENTAL SECTION

General Procedures. All chemicals were purchased from commercial sources and used as received. 4-Amino-3,5-bis(chloromethyl)-triazole·HCl was prepared as described previously.[13]

Elemental analyses were carried out by the Campbell Microanalytical Laboratory at the University of Otago. Infrared spectra were recorded over the range 4000−400 cm^{-1} by ATR using a Bruker alpha P. Magnetic data were recorded over the range 300−4.2 K with a Quantum Design MPMS5 SQUID magnetometer (complexes **2**−**5** and **7**) or a Quantum Design PPMS equipped with a vibrating sample mount (complex **6**) with an applied field of 1 T at Industrial Research Limited (IRL). ESI mass spectra were recorded on a Bruker MicrOTOF$_Q$ spectrometer by Mr. Ian Stewart. ^{1}H and ^{13}C NMR spectra were recorded on either a Varian INOVA-500 or Varian INOVA-300 spectrometer at 25 °C.

^{57}Fe Mössbauer spectra were recorded at Otago on a low field Mössbauer spectroscopy system from SEE Co. (Science Engineering & Education Co., MN) by Dr. Guy N. L. Jameson, and all parameters are given relative to the centroid of the spectrum of iron foil measured at room temperature.

X-ray data were collected with a Bruker APEX II area detector diffractometer at the University of Otago (Table 4) using graphite-monochromated Mo−Kα radiation (λ = 0.71073 Å). The data were corrected for Lorentz and polarization effects and semiempirical absorption corrections (SCALE) were applied. The structures were solved by direct methods (SHELXS-97) and refined against all F^2 data (SHELXL-97).[24] Hydrogen atoms, except those attached to nitrogen and oxygen atoms which were typically located from difference maps and the coordinates fixed, were inserted at calculated positions and rode on the atoms to which they were attached. All non-hydrogen atoms were

Table 4. Crystallographic Parameters for [2]·2MeOH·H_2O (at 293 and 90 K), [5]·$^3/_4$IPA·H_2O (at 90 K) and [7]·1.6MeOH·0.4H_2O (at 90 K)

	$[Fe_2(\mathbf{PMAT})_2]Cl_4\cdot 2MeOH\cdot H_2O$	$[Fe_2(\mathbf{PMAT})_2]Cl_4\cdot 2MeOH\cdot H_2O$	$[Fe_2(\mathbf{PMAT})_2](CF_3SO_3)_4\cdot {}^3/_4IPA\cdot H_2O$	$[Fe_2(\mathbf{PMAT})_2](C_{16}SO_3)_4\cdot 1.6MeOH\cdot 0.4H_2O$
	[2]·2MeOH·H_2O	**[2]·2MeOH·H_2O**	**[5]·$^3/_4$IPA·H_2O**	**[7]·1.6MeOH·0.4H_2O**
empirical formula	$C_{34}H_{50}C_{l4}Fe_2N_{16}O_3$	$C_{34}H_{50}C_{l4}Fe_2N_{16}O_3$	$C_{38.25}H_{48}F_{12}Fe_2N_{16}O_{13.75}S_4$	$C_{97.60}H_{179.20}Fe_2N_{16}O_{14}S_4$
M_r	984.40	984.40	1419.87	2040.91
crystal system	triclinic	triclinic	monoclinic	triclinic
space group	$P\bar{1}$	$P\bar{1}$	$P2_1/c$	$P\bar{1}$
a [Å]	9.736(4)	11.598(2)	16.112(2)	10.609(6)
b [Å]	10.067(5)	13.741(3)	20.052(2)	11.020(6)
c [Å]	11.841(5)	15.781(4)	17.618(3)	24.228(18)
α [deg]	79.413(13)	64.688(12)	90	97.49(4)
β [deg]	83.020(14)	87.483(14)	91.810(6)	97.39(4)
γ [deg]	71.643(12)	67.086(12)	90	105.03(3)
V [Å^3]	1080.2(8)	2071.4(8)	5689.1(14)	2673(3)
Z	1	2	4	1
T [K]	293(2)	90(2)	91(2)	90(2)
$\rho_{calcd.}$[g/cm^3]	1.513	1.578	1.658	1.268
μ [mm^{-1}]	0.974	1.016	0.770	0.416
F(000)	510	1020	2894	1105
crystal size [mm]	0.20 × 0.12 × 0.08	0.20 × 0.12 × 0.08	0.40 × 0.20 × 0.20	0.32 × 0.10 × 0.02
θ range for data collection [deg]	2.58 to 26.53	1.44 to 26.67	2.34 to 25.00	1.99 to 25.00
reflections collected	8641	20220	31905	38943
independent reflections	4342	8279	9977	9386
R(int)	0.1253	0.0899	0.1098	0.1254
max. and min transmission	1.000 and 0.369	1.0000 and 0.727578	0.7454 and 0.6492	1.000 and 0.7110
data/restraints/parameters	4342/0/274	8279/0/534	9977/31/806	9386/2/627
GOF (F^2)	0.924	0.942	1.061	0.985
R_1 [$I > 2\sigma(I)$]	0.0770	0.0630	0.0944	0.0790
wR_2 [all data]	0.2206	0.2251	0.2981	0.2517
max/min res. e density [e Å^{-3}]	0.412 and −0.473	0.942 and −1.346	1.291 and −1.453	0.491 and −0.426

made anisotropic. Any deviation from this is stated in the relevant cif file. CCDC 780520 and 780521 ([2]·**2MeOH·H_2O** at 90 and 293 K), CCDC 780522 ([5]·$^3/_4$**IPA·H_2O** at 91 K), CCDC 780519 ([7]·**1.6MeOH·0.4H_2O** at 90 K) contain the supplementary crystallographic data for this paper. These data can be obtained free of charge from The Cambridge Crystallographic data Centre via www.ccdc.cam.ac.uk/data_request/cif.

*4-Amino-3,5-bis{[(2-pyridylmethyl)amino]methyl}-4H-1,2,4-triazole (**PMAT**).* To a very pale yellow solution of 2-(aminomethyl)-pyridine (1.62 g, 15.0 mmol) in CH_3CN (125 mL) was added solid sodium carbonate (2.65 g, 25.0 mmol). The resulting suspension was heated to 60 °C, at which temperature solid 4-amino-3,5,-bis(chloromethyl)-1,2,4-triazole hydrochloride (1.09 g, 5.00 mmol) was added and the mixture heated to 60 °C for 4 h, during which time the suspension turned from pale yellow to orange-brown. The mixture was allowed to cool to room temperature, filtered to remove a white precipitate, and the resulting clear solution evaporated to dryness under reduced pressure, giving a dark brown oil. This was purified by column chromatography (alumina, 5:1 ethanol:methanol) to give **PMAT** as an essentially pure orange oil, containing a trace of 2-(aminomethyl)-pyridine. This could be used in complexation reactions without problems. Yield: 1.57 g (97%). Mass spectral and NMR data were consistent with those previously reported.

*[Fe^{II}_2(**PMAT**)$_2$](BF$_4$)$_4$ (**1**).* To an orange-brown solution of crude **PMAT** (200 mg, 0.61 mmol) in dry methanol (20 mL) was added a pale green solution of $Fe(BF_4)_2\cdot 6H_2O$ (207 mg, 0.61 mmol) in 10 mL of dry methanol. The resulting brown solution was left to stir for 30 min during which time a pale precipitate formed. This was filtered and dried thoroughly in vacuo to give 266 mg of a pale yellow powder (78%). Found: C, 34.48; H, 3.77; N, 20.01 Calc. for $[Fe^{II}_2(\mathbf{PMAT})_2](BF_4)_2$ (1107.69 g mol^{-1}): C, 34.70; H, 3.64; N, 20.23.

*[Fe^{II}_2(**PMAT**)$_2$]Cl$_4$·4H$_2$O ([**2**]·4H$_2$O).* To an orange-brown solution of crude **PMAT** (130 mg, 0.40 mmol) in methanol (20 mL) was added a green solution of $FeCl_2\cdot 4H_2O$ (80 mg, 0.40 mmol) in 10 mL of methanol. The resulting pale yellow-brown solution was stirred for 1 h before being subjected to vapor diffusion of diethyl ether which yielded 63 mg of a yellow-brown powder (30%). This was then suspended in MeCN/DMF (4:1) and stirred for 4 h before the small amount of insoluble brown material was filtered. The filtrate was subjected to vapor diffusion of diethyl ether, resulting in a pale yellow-brown powder (50 mg). Found: C, 36.73; H, 4.11; N, 20.98 Calc. for $[Fe^{II}_2(\mathbf{PMAT})_2]Cl_4\cdot 4H_2O$ (1045.24 g mol^{-1}): C, 36.77; H, 4.63; N, 21.44. IR (ATR) 3227, 1605, 1571, 1480, 1333, 1094, 1053, 825, 765, 647, 403 cm^{-1}.

*[Fe^{II}_2(**PMAT**)$_2$](CF$_3$SO$_3$)$_4$·H$_2$O ([**5**]·H$_2$O).* $[Fe^{II}_2(\mathbf{PMAT})_2](BF_4)_4$ (100 mg, 0.09 mmol) was dissolved in 20 mL of water with slight heating to give a yellow solution. To this yellow solution was added an excess of the sodium trifluoromethanesulfonate (155 mg, 0.9 mmol). Isopropanol (20 mL) was added to the resulting yellow/brown solution. After 3 days in the refrigerator large colorless crystals formed

dx.doi.org/10.1021/ic200308k |*Inorg. Chem.* 2011, 50, 4586–4597

(50 mg, 41%). Found: C, 31.68; H, 3.21; N, 16.52 Calc. for $[Fe^{II}_2(\mathbf{PMAT})_2](CF_3SO_3)_4 \cdot H_2O$: C, 31.45; H, 3.08; N, 16.30. IR (ATR) 3280, 2971, 1609, 1442, 1248, 1224, 1152, 1026, 761, 634, 573, 517 cm^{-1}.

General Anion Exchange Procedure for the Preparation of $[Fe^{II}_2(PMAT)_2](X)_4$ where X = PF_6, SbF_6, $B(PhF)_4$. $[Fe^{II}_2(\mathbf{PMAT})_2](BF_4)_4$ (100 mg, 0.09 mmol) was dissolved in 20 mL of water with slight heating to give a yellow solution. To this yellow solution was added an excess of the sodium (ammonium in the case of PF_6) adduct of the desired counteranion, resulting in the precipitation of pale powders of the desired complexes. These were subsequently recrystallized from MeCN/DMF.

$[Fe^{II}_2(\mathbf{PMAT})_2](PF_6)_4$ ($[\mathbf{3}]$). The crude powder was obtained as a pale off white solid (72 mg, 60%) and recrystallized from a 4:1 MeCN/DMF solvent mixture to give 55 mg of a crystalline colorless solid. Found: C, 28.80; H, 3.25; N, 17.01 Calc. for $[Fe^{II}_2(\mathbf{PMAT})_2](PF_6)_4$ (1340.33 g mol^{-1}): C, 28.68; H, 3.01; N, 16.72. IR (ATR) 1677, 1609, 1444, 828, 739, 649, 555, 414 cm^{-1}.

$[Fe^{II}_2(\mathbf{PMAT})_2](SbF_6)_4 \cdot 2H_2O$ ($[\mathbf{4}] \cdot 2H_2O$). The crude powder was obtained as a pale slightly yellow solid (88 mg, 56%) and recrystallized from a 4:1 MeCN/DMF solvent mixture to give 48 mg of a microcrystalline off-white solid. Found: C, 22.12; H, 2.47; N, 12.58 Calc. for $[Fe^{II}_2(\mathbf{PMAT})_2](SbF_6)_4 \cdot 2H_2O$ (1739.46 g mol^{-1}): C, 22.10; H, 2.55; N, 12.88. IR (ATR) 3343, 1610, 1443, 1161, 1057, 1024, 891, 768, 659, 626 cm^{-1}.

$[Fe^{II}_2(\mathbf{PMAT})_2](B(PhF)_4)_4 \cdot {}^1/_2MeCN$ ($[\mathbf{6}] \cdot {}^1/_2MeCN$). The crude powder was obtained as a pale off-white solid (113 mg, 54%) and recrystallized from a 4:1 MeCN/DMF solvent mixture to give 84 mg of a microcrystalline off-white solid. Found: C, 66.28; H, 4.36; N, 9.90 Calc. for $[Fe^{II}_2(\mathbf{PMAT})_2](B(C_6H_4F)_4)_4 \cdot 1/2MeCN$ (2345.76 g mol^{-1}): C, 66.05; H, 4.53; N, 9.85. IR (ATR) 1580, 1487, 1438, 1209, 1155, 812, 762, 646, 549, 413 cm^{-1}.

$[Fe^{II}_2(\mathbf{PMAT})_2](C_{16}SO_3)_4 \cdot 2H_2O$ ($[\mathbf{7}] \cdot 2H_2O$). **PMAT** (0.167 g, 0.51 mmol) was dissolved in MeOH (10 mL) and the solution thoroughly degassed via consecutive vacuum/argon purges. Without exposure to air, this solution was added a solution of $[Fe^{II}(OH_2)_2(C_{16}SO_3)_2]$ (0.361 g, 0.51 mmol) in thoroughly degassed MeOH (50 mL), resulting in the precipitation of a yellow-brown solid. The suspension was stirred for a further 5 min before being filtered under argon yielding $[Fe^{II}_2(\mathbf{PMAT})_2](C_{16}SO_3)_4 \cdot 2H_2O$ (0.234 g, 45%). Found: C, 56.83; H, 8.54; N, 11.31; S, 6.17 Calc. for $[Fe^{II}_2(\mathbf{PMAT})_2](C_{16}SO_3)_4 \cdot 2H_2O$: C, 57.12; H, 8.79; N, 11.10; S, 6.35. IR (ATR) 3444, 3267, 2917, 2850, 1609, 1467, 1440, 1173, 1096, 1036, 762, 720, 604, 524 cm^{-1}.

■ ASSOCIATED CONTENT

Supporting Information. Crystallographic data in CIF format, additional crystal structure diagrams (Figures S1−S8) and tables of hydrogen bonds (Tables S1−S4), magnetic moment vs temperature plots (Figures S9−S13), comparison of % HS obtained from magnetic and Mössbauer data (Table S5, Figure S14), and experimental details for recording the Mössbauer spectra. This material is available free of charge via the Internet at http://pubs.acs.org.

■ AUTHOR INFORMATION

Corresponding Author
*E-mail: sbrooker@chemistry.otago.ac.nz.

■ ACKNOWLEDGMENT

This work was supported by grants from the University of Otago, the MacDiarmid Institute for Advanced Materials and Nanotechnology, and the RSNZ Marsden Fund. We are grateful to Professor Martin Albrecht (University College Dublin, previously University of Fribourg) and Claudio Gandolfi (University of Fribourg) for testing the ability of $[\mathbf{7}] \cdot \mathbf{2H_2O}$ to form a Langmuir film, and to Dr. Victoria A. Milway (Brooker group) for helpful discussions regarding our magnetic data. This paper is dedicated to Mrs. Marianne Dick on the occasion of her retirement from the Campbell Microanalytical Laboratory.

■ REFERENCES

(1) Haasnoot, J. G. *1,2,4-Triazoles as ligands for iron(II) high spin-low spin crossovers*; Kluwer Academic Publishers: Dordrecht, The Netherlands, 1996; pp 299−321; Lavrenova, L. G.; Larionov, S. V. *Russ. J. Coord. Chem.* **1998**, *24*, 379–395. Kahn, O. *Chem. Br.* **1999**, *2*, 24–27. Kitchen, J. A.; Brooker, S. *Coord. Chem. Rev.* **2008**, *252*, 2072–2092.

(2) Kahn, O.; Codjovi, E. *Phil. Trans. R. Soc. London, Ser. A* **1996**, *354*, 359–379. van Koningsbruggen, P. J. *Top. Curr. Chem.* **2004**, *233*, 123–149.

(3) Constable, E. C.; Baum, G.; Bill, E.; Dyson, R.; van Eldik, R.; Fenske, D.; Kaderli, S.; Morris, D.; Neubrand, A.; Neuburger, M.; Smith, D. R.; Wieghardt, K.; Zehnder, M.; Zuberbühler, A. D. *Chem.—Eur. J.* **1999**, 498–508. Nakano, K.; Suemura, N.; Yoneda, K.; Kawata, S.; Kaizaki, S. *Dalton Trans.* **2005**, 740–743.

(4) Zhang, W.; Zhao, F.; Liu, T.; Yuan, M.; Wang, Z.-M.; Gao, S. *Inorg. Chem.* **2007**, *46*, 2541–2555.

(5) Leita, B. A.; Neville, S. M.; Halder, G. J.; Moubaraki, B.; Kepert, C. J.; Létard, J.-F.; Murray, K. S. *Inorg. Chem.* **2007**, *46*, 8784–8795.

(6) Quesada, M.; Prins, F.; Bill, E.; Kooijman, H.; Gamez, P.; Roubeau, O.; Spek, A. L.; Haasnoot, J. G.; Reedijk, J. *Chem.—Eur. J.* **2008**, *14*, 8486–8499. Drtu, M. M.; Rotaru, A.; Gillard, D.; Linares, J.; Codjovi, E.; Tinant, B.; Garcia, Y. *Inorg. Chem.* **2009**, *48*, 7838–7852.

(7) Bonnet, S.; Molnár, G.; Costa, J. S.; Siegler, M. A.; Spek, A. L.; Bousseksou, A.; Fu, W.-T.; Gamez, P.; Reedijk, J. *Chem. Mater.* **2009**, *21*, 1123–1136.

(8) Weber, B. *Coord. Chem. Rev.* **2009**, *253*, 2432–2449.

(9) Brooker, S.; Kitchen, J. A. *Dalton Trans.* **2009**, 7331–7340, and front cover image.

(10) Klingele, M. H.; Moubaraki, B.; Cashion, J. D.; Murray, K. S.; Brooker, S. *Chem. Commun.* **2005**, 987–989.

(11) Grunert, C. M.; Reiman, S.; Spiering, H.; Kitchen, J. A.; Brooker, S.; Gütlich, P. *Angew. Chem., Int. Ed.* **2008**, *47*, 2997–2999.

(12) Bhattacharjee, A.; Ksenofontov, V.; Kitchen, J. A.; White, N. G.; Brooker, S.; Gütlich, P. *Appl. Phys. Lett.* **2008**, *92*, 174104.

(13) Klingele, M. H.; Moubaraki, B.; Murray, K. S.; Brooker, S. *Chem.—Eur. J.* **2005**, *11*, 6962–6973.

(14) Fujigaya, T.; Jiang, D.-L.; Aida, T. *Chem. Asian J.* **2007**, *2*, 106–113.

(15) White, N. G.; Feltham, H. L. C.; Gandolfi, C.; Albrecht, M.; Brooker, S. *Dalton Trans.* **2010**, *39*, 3751–3758.

(16) Noble, A.; Olguín, J.; Clérac, R.; Brooker, S. *Inorg. Chem.* **2010**, *49*, 4560–4569.

(17) White, N. G.; Kitchen, J. A.; Brooker, S. *Eur. J. Inorg. Chem.* **2009**, 1172–1180.

(18) (a) Drew, M. G. B.; Harding, C. J.; McKee, V.; Morgan, G. G.; Nelson, J. *J. Chem. Soc., Chem. Commun.* **1995**, 1035–1038. (b) Nelson, J.; McKee, V.; Morgan, G. *Prog. Inorg. Chem.* **1998**, *47*, 167–317. (c) Guionneau, P.; Brigouleix, C.; Barrans, Y.; Goeta, A. E.; Letard, J.-F.; Howard, J. A. K.; Gaultier, J.; Chassaeu, D. *C. R. Acad. Sci. Paris, Chim.* **2001**, *4*, 161–171.

(19) Guionneau, P.; Marchivie, M.; Bravic, G.; Letard, J.-F.; Chasseau, D. *Top. Curr. Chem.* **2004**, *234*, 97–128.

(20) Halder, G. J.; Kepert, C. J.; Moubaraki, B.; Murray, K. S.; Cashion, C. S. *Science* **2002**, *298*, 1762–1765. Bartel, M.; Absmeier, A.; Jameson, G. N. L.; Werner, F.; Kato, K.; Takata, M.; Boca, R.; Hasegawa, M.; Mereiter, K.; Caneschi, A.; Linert, W. *Inorg. Chem.* **2007**, *46* (10), 4220–4229.

(21) Kitchen, J. A.; White, N. G.; Gandolfi, C.; Albrecht, M.; Jameson, G. N. L.; Tallon, J. L.; Brooker, S. *Chem. Commun.* **2010**, *46*, 6464–6466.

(22) Greenwood, N. N.; Gibb, T. C. *Mössbauer spectroscopy*; Chapman and Hall Ltd: London, 1971; p 659.

(23) Dosser, R. J.; Eilbeck, W. J.; Underhill, A. E.; Edwards, P. R.; Johnson, C. E. *J. Chem. Soc. A* **1969**, 810–816. Berna, I.; Jensen, l. M.; Jensen, K.; McKenzie, C. J.; Toftlund, H.; Tuchagues, J.-P. *J. Chem. Soc., Dalton Trans.* **1995**, 3667–3675. Psomas, G.; Brefuel, N.; Dahan, F.; Tuchagues, J.-P. *Inorg. Chem.* **2004**, *43*, 4590–4594.

(24) Sheldrick, G. M. *Acta Crystallogr., Sect. A* **2008**, *A64*, 112–122.